ARL-TR-9416 • MAR 2022

A Model for a Kolsky Bar Experiment: Application to Experiment Design

by Daniel Casem

NOTICES

Disclaimers

The findings in this report are not to be construed as an official Department of the Army position unless so designated by other authorized documents.

Citation of manufacturer's or trade names does not constitute an official endorsement or approval of the use thereof.

Destroy this report when it is no longer needed. Do not return it to the originator.

ARL-TR-9416 ● MAR 2022

A Model for a Kolsky Bar Experiment: Application to Experiment Design

Daniel Casem
DEVCOM Army Research Laboratory

REPORT DOCUMENTATION PAGE

Form Approved
OMB No. 0704-0188

1. REPORT DATE *(DD-MM-YYYY)*	2. REPORT TYPE	3. DATES COVERED (From - To)
March 2022	Technical Report	1 September–1 December 2021

4. TITLE AND SUBTITLE
A Model for a Kolsky Bar Experiment: Application to Experiment Design

5a. CONTRACT NUMBER

5b. GRANT NUMBER

5c. PROGRAM ELEMENT NUMBER

6. AUTHOR(S)
Daniel Casem

5d. PROJECT NUMBER

5e. TASK NUMBER

5f. WORK UNIT NUMBER

7. PERFORMING ORGANIZATION NAME(S) AND ADDRESS(ES)
DEVCOM Army Research Laboratory
ATTN: FCDD-RLW-TC
Aberdeen Proving Ground, MD 21005

8. PERFORMING ORGANIZATION REPORT NUMBER
ARL-TR-9416

9. SPONSORING/MONITORING AGENCY NAME(S) AND ADDRESS(ES)

10. SPONSOR/MONITOR'S ACRONYM(S)

11. SPONSOR/MONITOR'S REPORT NUMBER(S)

12. DISTRIBUTION/AVAILABILITY STATEMENT
Approved for public release: distribution unlimited.

13. SUPPLEMENTARY NOTES

14. ABSTRACT
Solutions to the one-dimensional wave equation along with simple descriptions of the sample's mechanical response are used to analyze a Kolsky bar experiment. If the approximate sample behavior is known, the experiment can be predicted in advance. This allows one to design the experiment (choice of bar and sample geometry, striker speed, instrumentation, etc.) to obtain the desired specimen deformation (rate, final strain, etc.). The effects of pulse shapers and tapered projectiles are included.

15. SUBJECT TERMS
split Hopkinson pressure bar, Kolsky bar, high-rate testing, wave propagation, mechanical testing

16. SECURITY CLASSIFICATION OF:			17. LIMITATION OF ABSTRACT	18. NUMBER OF PAGES	19a. NAME OF RESPONSIBLE PERSON
a. REPORT	b. ABSTRACT	c. THIS PAGE			Daniel Casem
Unclassified	Unclassified	Unclassified	UU	30	19b. TELEPHONE NUMBER (Include area code) (410) 306-0972

Contents

List of Figures

List of Tables

1. Introduction

Kolsky bar, or split Hopkinson pressure bar, experiments are the most commonly used method to measure the constitutive response of materials at strain rates in the range of 1000 to 10,000/s. Overviews can be found in literature,[1–5] and it is assumed the reader is familiar with the basic operation.

This report focuses on the compression arrangement, but much of what is discussed applies to tension and torsion as well. Figure 1 shows the most common setup. The input and output bars are identical, with length L, wave speed c, elastic modulus E, and cross-sectional area A_b. Each is instrumented with strain gages at the midpoint. The strain gages measure the input, reflected, and output pulses. These strain signals are denoted as ε_i, ε_r, and ε_o.* Because the measurements are made at the midpoints, the measured signals must be time-shifted to the times they act at the sample interfaces, and the equations in this section assume this has been done. The time shifting may also include a dispersion correction,[6–9] but in this report dispersion effects are neglected. The sample is assumed to be free from inertial effects and in a state of quasi-static equilibrium. These two assumptions lead to the simplification that

$$\epsilon_o = \epsilon_i + \epsilon_r \tag{1}$$

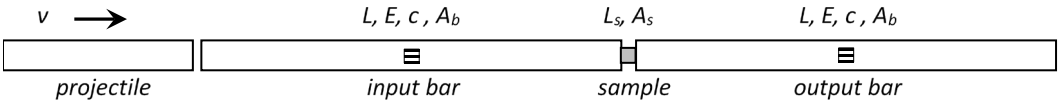

Fig. 1 A typical compression bar

The striker (same material and area as the bars) impacts at a speed v, and must be somewhat less than half the length of the input bar so that the input pulse and reflection can be measured separately. Similarly, the output pulse must be short enough as to not interfere with its own reflection from the free-end, or else a more complex analysis is needed. The initial length and area of the sample are L_s and A_s. Engineering stress, strain rate, and strain for the sample can then be found.

$$\sigma_s = \epsilon_o E \frac{A_b}{A_s} \tag{2}$$

$$\dot{\epsilon}_s = \epsilon_r \frac{c}{L_s} \tag{3}$$

$$\epsilon_s = \int \dot{\epsilon}_s \, dt \tag{4}$$

* Stress and strain in this report are assumed positive in compression.

Thus the sample stress–strain curve is determined from the measured reflected and output pulses. In theory, since the input pulse is also known, by Eq. 1 only one of these is needed to determine the specimen response although this is rarely done in practice.

Conversely, if the sample stress–strain behavior is known, the sample's entire deformation history can be determined for a given set of bar properties and input pulse. Manipulating Eqs. 1–4 to solve for strain rate gives the following:

$$\dot{\epsilon}_s = \frac{c}{L_s}\left(\frac{\sigma_s A_s}{E A_b} - \epsilon_i\right) \tag{5}$$

The sample strain, as a function of time, can then be found by time integration. Because the sample's constitutive behavior can be complicated, this is best done numerically. However, since the sample behavior is almost always known approximately in advance of actual testing, this provides a useful tool for designing Kolsky bar experiments. For example, it allows one to choose the bar parameters along with the input pulse to obtain the desired deformation (e.g., a constant strain rate and a particular final strain in the sample).[*] It will show whether the sample will be naturally recovered so that a postmortem analysis can be performed without the need for input bar momentum traps or stop rings to limit sample deformation. It can also help one decide what instrumentation should be used. For example, once the sample load history is known from Eq. 5, the output and reflected pulses can be determined from Eqs. 2 and 3. Will the signal be too weak in the output bar for a standard strain gage or must a semiconductor gage be used? Perhaps a more compliant bar (aluminum vs. steel) should be used, or a hollow one or one of a smaller diameter. Similarly, will the relative magnitudes of the stress waves in the input bar be suitable to determine force at the input bar–sample interface? All of these things can be considered prior to testing.

Of course, most research groups conduct some type of similar analysis to design experiments. The purpose of this report is to develop this idea in a general way. The bars can be of different materials and geometry, a pulse shaper or tapered striker may be used, and there are no limitations on the lengths of the pulses or reverberations/overlap of the key stress pulses. Examples are given with practical applications. This same framework can be used to provide boundary conditions for finite element models. This would allow a simulation of a dynamically loaded sample to be conducted without the need to include the bars in the mesh, although this possibility is not explored here.

[*] This was used by Casem[10] to determine the shape of the input pulse needed to result in a constant strain-rate experiment for a material with an approximately known constitutive response, and also to generate a stepped strain-rate loading.

The next section gives the d'Alembert solution[11,12] of the one-dimensional (1-D) wave equation for a single pressure bar loaded at each end. Section 3 rewrites this solution for the case of a standard compression bar: input and output bars where the loads are due to the striker bar and the sample. Two possible methods to describe the sample are given in Sections 4 and 5. Finally, Section 6 gives some examples of application. Readers should be aware that notation is only consistent within sections due to the large number of subscripts needed to describe the various topics. For example, P and v consistently refer to force and velocity, but the subscript i might in some cases refer to the *input* bar or an *initial* condition in others.

2. Behavior of a Single Pressure Bar

Figure 2 shows a single pressure bar loaded axially with compressive loads at each end. It is linear elastic and has wave speed c and impedance Z (product of wave speed, density, and cross-sectional area). The loads $P_A(t)$ and $P_B(t)$ are known. It could be an input bar, in which case P_A would be the force due to the striker and the force P_B due to the sample. It could be an output bar, where P_A would be due to the sample and P_B would be zero, for the case of a free end. It could also be a striker bar, or a segment in a striker bar that had multiple segments. It could even be a momentum trap, either one used to back up an output bar or a hollow momentum trap used to arrest the reflection in a flanged input bar. The only restrictions are that there are no loads applied within the two ends and that dispersion is negligible.

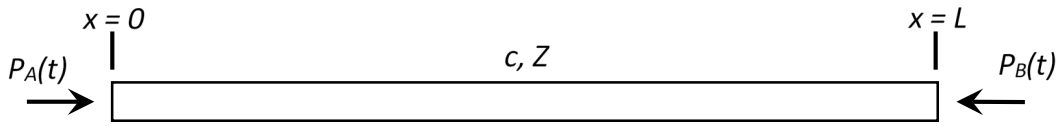

Fig. 2 A general bar loaded arbitrarily at both ends

The velocity and force at any point along the bar is the sum of the components due to two wave trains, F, moving in the direction of positive x, and G, moving in the direction of negative x.

$$v(x,t) = F\left(\frac{x}{c} - t\right) + G\left(\frac{x}{c} + t\right) \tag{6}$$

$$\frac{P(x,t)}{Z} = F\left(\frac{x}{c} - t\right) - G\left(\frac{x}{c} + t\right) \tag{7}$$

Applying the boundary conditions $P(0,t) = P_A(t)$ and $P(L,t) = P_B(t)$ gives F and G.

$$\frac{P_B(t)}{Z} - \frac{P_A\left(t-\frac{L}{c}\right)}{Z} = G\left(t-\frac{L}{c}\right) - G\left(t+\frac{L}{c}\right) \tag{8}$$

$$\frac{P_B(t)}{Z} - \frac{P_A\left(t+\frac{L}{c}\right)}{Z} = F\left(-t+\frac{L}{c}\right) - F\left(-t-\frac{L}{c}\right) \tag{9}$$

This allows F and G to be determined from the loads applied to the ends. Once this has been done, the solution is fully known and the force and velocity at any point on the bar can be determined for all time, regardless of superimposed reflections, by using Eqs. 6 and 7.

3. Applications to a Compressive Kolsky Bar

Figure 3 shows a simple compression bar, with no momentum trap. The sample, not necessarily in equilibrium, exerts a force on each bar as it is deformed. In this way, the deformation of the sample is coupled to the wave mechanics in the bars. The input force, essentially the input pulse generated by some type of striker with or without a pulse shaper, must be known. The equations in the preceding section can be applied to both bars, independently (note the independent axes x and x'). In this case, the loads $P_p(t)$ and $P_{s1}(t)$ act at the ends of the input bar. The load $P_{s2}(t)$ acts on the output bar and the other end is free.

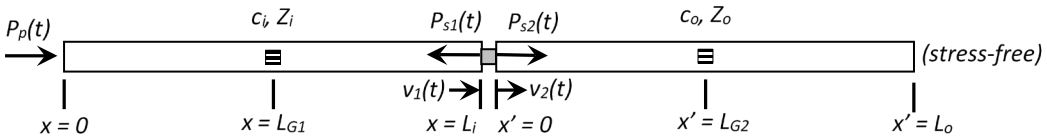

Fig. 3 A more general compressive Kolsky bar

Equations 8 and 9 apply to each bar. This allows F_i, G_i, and F_o, and G_o to be determined (i.e., $F(x/c-t)$ and $G(x/c+t)$ for the input and output bars). Because of the time translations, this can only be done if there is some initial time before which there are no waves; fortunately, this is the case for a Kolsky bar prior to projectile impact. The equations are as follows.

$$\frac{P_{s1}(t)}{Z_i} - \frac{P_p\left(t-\frac{L_i}{c_i}\right)}{Z_i} = G_i\left(t-\frac{L_i}{c_i}\right) - G_i\left(t+\frac{L_i}{c_i}\right) \tag{10}$$

$$\frac{P_{s1}(t)}{Z_i} - \frac{P_p\left(t+\frac{L_i}{c_i}\right)}{Z_i} = F_i\left(-t+\frac{L_i}{c_i}\right) - F_i\left(-t-\frac{L_i}{c_i}\right) \tag{11}$$

$$-\frac{P_{s2}\left(t-\frac{L_o}{c_o}\right)}{Z_o} = G_o\left(t-\frac{L_o}{c_o}\right) - G_o\left(t+\frac{L_o}{c_o}\right) \tag{12}$$

$$-\frac{P_{s2}\left(t+\frac{L_o}{c_o}\right)}{Z_o} = F_o\left(-t+\frac{L_o}{c_o}\right) - F_o\left(-t-\frac{L_o}{c_o}\right) \tag{13}$$

Equations 6 and 7 can be rewritten for each bar; that is, the velocity at any point on the input and output bars can be expressed as follows.

$$v_i(x,t) = F_i\left(\frac{x}{c_i} - t\right) + G_i\left(\frac{x}{c_i} + t\right) \tag{14}$$

$$v_o(x',t) = F_o\left(\frac{x'}{c_o} - t\right) + G_o\left(\frac{x'}{c_o} + t\right) \tag{15}$$

Similar equations can be written for $P_i(x,t)$ and $P_o(x',t)$, the forces at any point on the input and output bars.

$$\frac{P_i(x,t)}{Z_i} = F_i\left(\frac{x}{c_i} - t\right) - G_i\left(\frac{x}{c_i} + t\right) \tag{16}$$

$$\frac{P_o(x,t)}{Z_o} = F_o\left(\frac{x}{c_o} - t\right) - G_o\left(\frac{x}{c_o} + t\right) \tag{17}$$

Equations 14 and 15 can then be used to determine the motion of the interfaces between the samples and the bars, labeled v_1 and v_2 in Fig. 3.

$$v_1(t) = v_i(L,t) = F_i\left(\frac{L_i}{c_i} - t\right) + G_i\left(\frac{L_i}{c_i} + t\right) \tag{18}$$

$$v_2(t) = v_o(0,t) = F_o(-t) + G_o(t) \tag{19}$$

The same equations can be used to determine velocity or force at any other point in the bar, for example at a gage location ($x = L_{G1}$ or $x' = L_{G2}$). Of more interest is the strain at the gage locations, since this is what is typically measured. Strain is easily related to axial force ($\varepsilon = P/(EA)$), so the strain at each gage location can be found.

$$\epsilon_i(L_{G1},t) = \frac{P_i(L_{G1},t)}{A_i E_i} = \frac{1}{c_i}\left(F_i\left(\frac{L_{G1}}{c_i} - t\right) - G_i\left(\frac{L_{G1}}{c_i} + t\right)\right) \tag{20}$$

$$\epsilon_o(L_{G2},t) = \frac{P_o(L_{G2},t)}{A_o E_o} = \frac{1}{c_o}\left(F_o\left(\frac{L_{G2}}{c_o} - t\right) - G_o\left(\frac{L_{G2}}{c_0} + t\right)\right) \tag{21}$$

Thus the entire solution to the wave equation in both bars can be found, provided the sample response can be related to the behavior of the bars. This is covered in the next section.

4. An Elastic-Plastic Sample

The sample can be represented in a number of ways. All that is needed in the present case is a reasonably accurate way to represent the forces exerted by the sample on the bars, and not a detailed description of the sample's mechanical behavior. An elastic-plastic behavior with a simple failure model will suffice. An identical approach can be used to model a pulse shaper. The sample mass is neglected (no

specimen inertia) and equilibrium is assumed, so the sample force P_s acts on each pressure bar in Fig. 3.

$$P_{s1} = P_{s2} = P_s \tag{22}$$

The flow force in the sample, P_{flow}, is related to the sample deformation by the following.

$$P_{flow} = A + B{\delta_p}^n \tag{23}$$

Here A, B, and n are constants, and δ_p is the plastic deformation of the sample. A is a yield force. The elastic deformation is linear.

$$P_e = k\delta_e \tag{24}$$

Here k is an elastic constant. A failure deformation can be defined, allowing the sample to fail completely and instantaneously.

$$P_s = 0 \text{ if } \delta_s > \delta_f \tag{25}$$

Here δ_s is the sample total deformation. It is the sum of the elastic and plastic parts.

$$\delta_s = \delta_e + \delta_p \tag{26}$$

This is valid for standard compression testing, where the sample is not loaded in tension. In a more general case, a sample might be loaded plastically in both tension and compression due to some complex load history. This equation could lead to the unrealistic situation of plastic strain decreasing, and a slightly more complex treatment would be needed.

There is no need to define a sample length, as everything can be calculated in terms of the relevant displacements. Figure 4 shows these quantities. The sample deformation is coupled to the bars and can be integrated numerically using the equations in Section 3. A simple contact algorithm is included to allow the sample to separate from the input bar, and no tension is permitted. In some experiments, it is useful to leave a small initial gap between the sample and one bar to avoid preloading the sample (e.g., indentation), so an initial gap δ_{gap} (*not* the instantaneous gap) is also shown in the figure. In most cases, this will be zero.

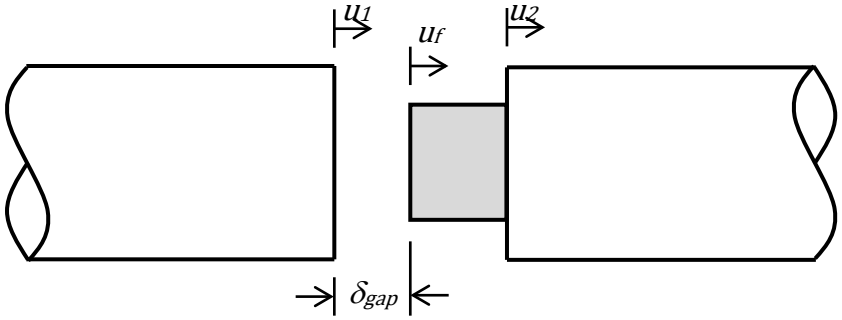

Fig. 4 A sample, fixed to the output bar, and an initial gap between it and the input bar

At the beginning of the time step, ${v_1}^t$ and ${v_2}^t$ are known from Eqs. 18 and 19. They are assumed constant throughout the time step. The displacements of each end of the bar at the end of the time step are found next.

$${u_1}^{t+\Delta t} = {u_1}^t + {v_1}^t \Delta t \tag{27}$$

$${u_2}^{t+\Delta t} = {u_2}^t + {v_2}^t \Delta t \tag{28}$$

For compression testing, the sample can be treated as fixed to the output bar but allowed to separate from the input bar. Since the sample is massless, there is no downside to this and it simplifies the contact treatment. As shown in Fig. 4, u_f is the displacement of the sample face. At the beginning of each time step, the assumption is made that the sample face is in contact with the input bar. If this results in a tensile force, there is no contact, and the actual u_f is determined such that the force in the sample is zero, allowing it to unload elastically and separate from the input bar. If it is in contact with the input bar, then

$${u_f}^{t+\Delta t} = {u_1}^{t+\Delta t} - \delta_{gap} \tag{29}$$

The force in the sample is next found using a radial return method. The sample deformation at any time is

$$\delta = {u_f}^t - {u_2}^t \tag{30}$$

since the sample is fixed to the output bar. The change in deformation for the current time step is

$$\Delta\delta = \left({u_f}^{t+\Delta t} - {u_2}^{t+\Delta t}\right) - \left({u_f}^t - {u_2}^t\right) = {u_f}^{t+\Delta t} - {u_f}^t - {v_2}^t \Delta t \tag{31}$$

A trial force is now found, assuming the sample deformation during this time step is elastic.

$${P_{trial}}^{t+\Delta t} = {P_s}^t + k\Delta\delta \tag{32}$$

The current flow force is also determined, assuming the new increment of deformation is entirely plastic.

$$P_{flow}{}^{t+\Delta t} = A + B\left(\delta_s{}^{t} - {P_s{}^{t}}/{k} + \Delta\delta\right)^{n} \tag{33}$$

There are three possibilities for $P_{trial}{}^{t+\Delta t}$. The first is $P_{trial}{}^{t+\Delta t} < 0$. This means the assumption that the input bar and sample were in contact was incorrect, and $u_f{}^{t+\Delta t}$ is adjusted so that the sample force is zero. This can be done by allowing the sample to unload (assumed elastic) and then solving for $u_f{}^{t+\Delta t}$ in Eq. 33 such that the trial force is zero.

$$u_f{}^{t+\Delta t} = u_f{}^{t} - {P_s{}^{t}}/{k} + v_2{}^{t}\Delta t \tag{34}$$

This value is used for the updated position of the sample face instead of Eq. 29, and the forces on the ends of the bars are zero.

The next possibility is that the trial force from Eq. 32 is positive but less than the flow force. In this case, the deformation is elastic (possibly loading or unloading), and

$$P_s{}^{t+\Delta t} = P_{trial}{}^{t+\Delta t} \tag{35}$$

No adjustment is needed for $u_f{}^{t+\Delta t}$; the value given by Eq. 29 is correct. The final possibility is that $P_{trial}{}^{t+\Delta t}$ exceeds the flow force, and the force is simply returned to the yield surface.

$$P_s{}^{t+\Delta t} = P_{flow}{}^{t+\Delta t} \tag{36}$$

Again, $u_f{}^{t+\Delta t}$ does not need to be adjusted.

At this point, the sample surface motion and sample force have been determined, and the new forces are applied to the ends of the bars (Eqs. 10–13). New values of v_1 and v_2 (Eqs. 18 and 19) can be found and the process repeated. If at any time the sample deformation exceeds δ_f, the force is zero for all remaining time. In this formulation, there is no way for the input and output bars to contact directly, even after the sample has failed. The size of the time step, Δt, can be chosen somewhat arbitrarily depending on the required accuracy; this in turn can be confirmed by a standard convergence analysis.

5. Incompressible Plastic Flow with Johnson–Cook Strength

The sample behavior in the previous section can be replaced with any number of constitutive models that may be more convenient for a particular application. In this section, the sample is assumed to obey the Johnson–Cook[13] strength law and

undergo incompressible deformation. This is useful for a wide range of testing on metals. As discussed previously, the parameters for the sample should be approximately known, for example, from a low-rate test on a servo-hydraulic load-frame. The Johnson–Cook equation is as follows.

$$\tilde{\sigma}_s = \left(C_1 + C_2 \tilde{\epsilon}_p{}^n\right)\left(1 + C_3 \ln \frac{\dot{\tilde{\epsilon}}_p}{\dot{\tilde{\epsilon}}_{p,r}}\right)\left(1 - \left(\frac{T - T_r}{T_m - T_r}\right)^m\right) \tag{37}$$

Here the "~" accent denotes true stress and strain, as opposed to the engineering quantities. C_1, C_2, C_3, n, and m are all constants. $\dot{\tilde{\epsilon}}_{p,r}$ is a reference strain rate, T_r is a reference temperature, and T_m is the melting point. For incompressible flow in compression, true stress and strain are related to the engineering quantities by

$$\tilde{\sigma}_s = \sigma_s(1 - \tilde{\epsilon}_s) \tag{38}$$

$$\tilde{\epsilon}_s = -\ln(1 - \epsilon_s) \tag{39}$$

where

$$\epsilon_s = \frac{(u_f - u_2)}{L_0} \tag{40}$$

$$\sigma_s = \frac{P_s}{A_0} = \frac{P_{s1}}{A_0} = \frac{P_{s2}}{A_0} \tag{41}$$

Initial specimen dimensions (for a cylinder) are L_0 and $A_0 = \pi {d_0}^2/4$. Constant volume implies that they are related to the instantaneous values by

$$A_0 L_0 = A_i L_i \tag{42}$$

The elastic deformation is linear and E is the Young's modulus. The plastic deformation is adiabatic so that the sample temperature can be determined.

$$T = T_r + \frac{\beta}{\rho c_p} \int_0^{\epsilon_p} \sigma_s d\epsilon_p{}' \tag{43}$$

Here β is the fraction of plastic work converted into heat, ρ is the density of the sample, and c_p is its specific heat capacity.

This is everything needed to relate the sample deformation to the forces at the ends of the bars, following the same general algorithm described in Section 4. At the beginning of a time step, v_1 and v_2 (along with u_1 and u_2) are known. Contact is initially assumed, and the sample strain and sample strain rate can be determined. A trial force is calculated based on Eq. 32 where the deformation is assumed elastic according to the elastic modulus of the sample ($k = EA_i/L_i$). The checks on the trial force are applied, the actual sample force determined, and the sample face position updated accordingly. The only substantial difference is that the flow force is determined by the Johnson–Cook equation rather than Eq. 23. A fracture strain can be defined in a similar manner, that is,

$$\sigma_s = 0 \; for \; \epsilon_s > \epsilon_{fail} \tag{44}$$

6. Examples

The algorithms described in the preceding sections have been implemented into the commercial software Microsoft Excel. Inputs are the bar, striker, and specimen properties. Outputs are the stress and strain in the sample, along with the strain that is measured at the gage locations. Experiments can be designed iteratively, changing various bar properties or sample dimensions to achieve the desired effect. Some practical applications are given in this section.

6.1 Example 1: High-Rate Testing of 2139-T8 Aluminum

In this example, a laboratory is planning experiments on 2139-T8 aluminum. A set of Johnson–Cook parameters is available for this material.[14] The target strain rate (rate of true strain) is 2000/s. The laboratory has two sets of 20-mm-diameter bars; one set is made from a high-strength aluminum alloy (stronger than the sample) and the other from steel. The sample is quite large, L = D = 10 mm, and these dimensions cannot be changed for unspecified reasons. Which is the better choice for testing this material?

The aluminum bar is evaluated first. The parameters for the aluminum bar and the sample are given in Table 1. A time step of 0.0015 ms is used. Since this is a standard striker impact, the impedance of the striker matches that of the input bar, and the input pulse ($P_P(t)$ in Fig. 3) is a rectangular signal.

$$P_p(t) = \frac{1}{2} v_p Z_i \; for \; t \in \left[0, \frac{2L_s}{c_i}\right], 0 \; for \; all \; other \; times \tag{45}$$

Table 1 Input for an aluminum bar and a 2139-T8 aluminum sample

striker			input bar			output bar		
v_s =	40	*m/s*	c =	5000	*m/s*	c =	5000	*m/s*
L_s =	500	*mm*	L =	2000	*mm*	L =	2000	*mm*
			d =	20	*mm*	d =	20	*mm*
			ρ =	2800	kg/m^3	ρ =	2800	kg/m^3
			L_{gage} =	1000	*mm*	L_{gage} =	1000	*mm*

sample (Johnson-Cook strength)								
C_1 =	430	*MPa*	C_3 =	0		ρ =	2796	kg/m^3
C_2 =	650	*MPa*	$d\varepsilon_{p,r}/dt$ =	1	*1/s*	c_p =	900	J/kg-K
n =	0.5		T_r =	294.3	*K*	d =	10	*mm*
E =	73100	*MPa*	T_m =	933	*K*	L =	10	*mm*
ε_{fail} =	0.5		m =	1				

One could add a slight rise or decay time to be more realistic, but this is not done here. The predicted strain gage signals for this input data are given in Fig. 5a and the predicted stress–strain curve in Fig. 5b. Note the high striker speed, 40 m/s, needed to achieve the desired strain rate, and it is assumed that the bar will not yield. The true strain rate, also shown in Fig. 5b, is initially at 2000/s, but decays rapidly. The sample unloads at a final true strain of 0.3.

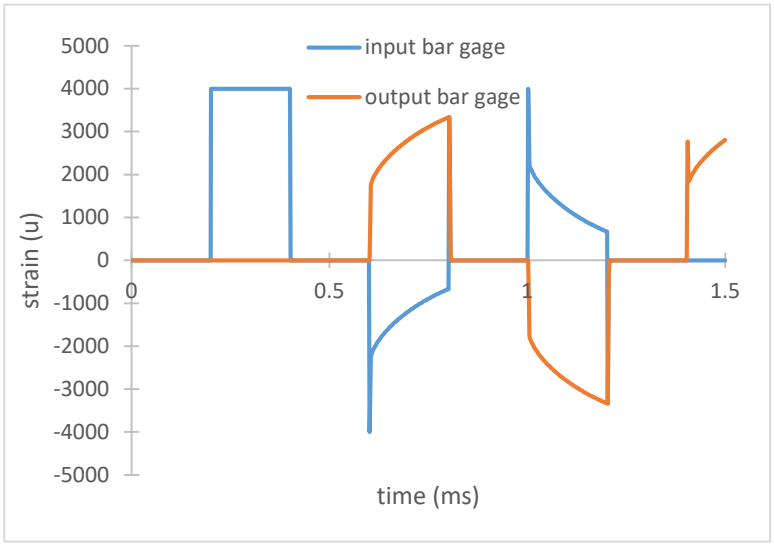

(a)

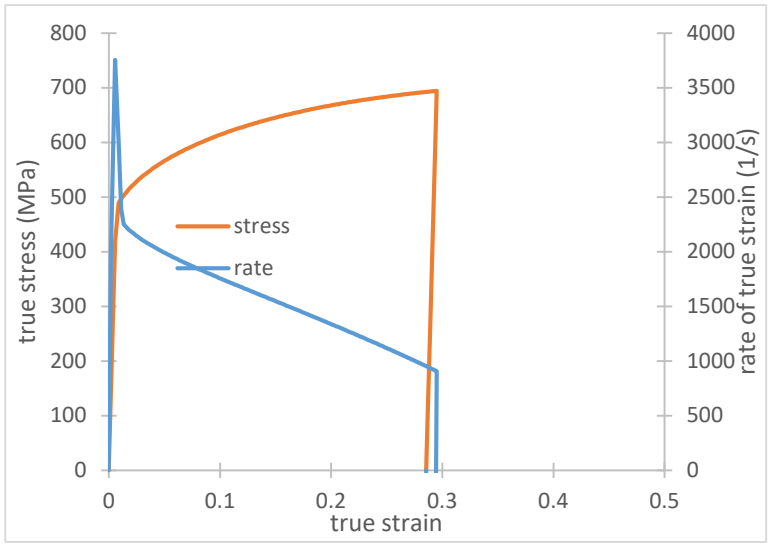

(b)

Fig. 5 (a) Strain signals for the test prediction using the aluminum bar (2800 kg/m^3) and a 500-mm-long striker at 40 m/s. (b) The stress–strain curves for the sample, along with the strain rate. Note the rate is not constant.

A prediction can next be made for the steel bars by changing the bar density to 8000 kg/m^3; the bars are otherwise identical. Because of the higher bar impedance, a striker speed of only 27 m/s is needed to achieve the desired strain rate. The strain signals and stress–strain curve are shown in Fig. 6. In this case, the strain rate is much more uniform, without the need for pulse shaping, and for this reason the steel bar would be a better choice for testing these samples. The final strain in the sample is higher (0.4), and if this was undesirable, a shorter striker could be used. How well the actual experiment will match these predictions depends mostly on how well the assumed Johnson–Cook parameters match the actual sample behavior.

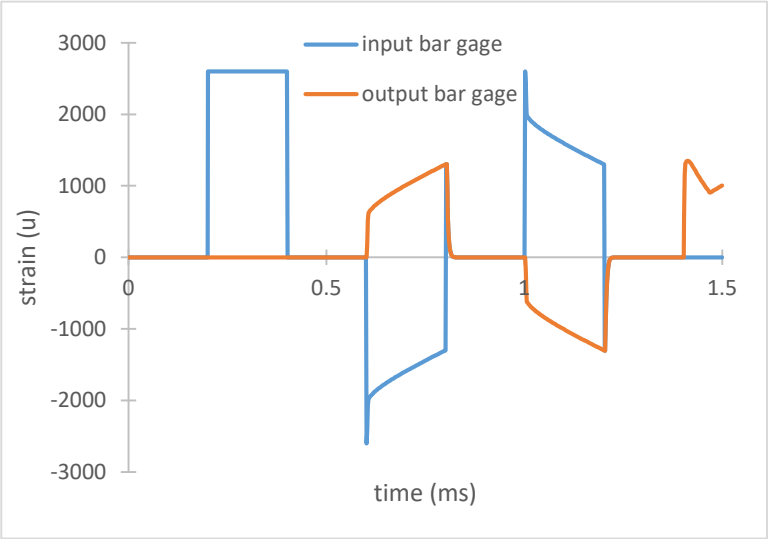

(a)

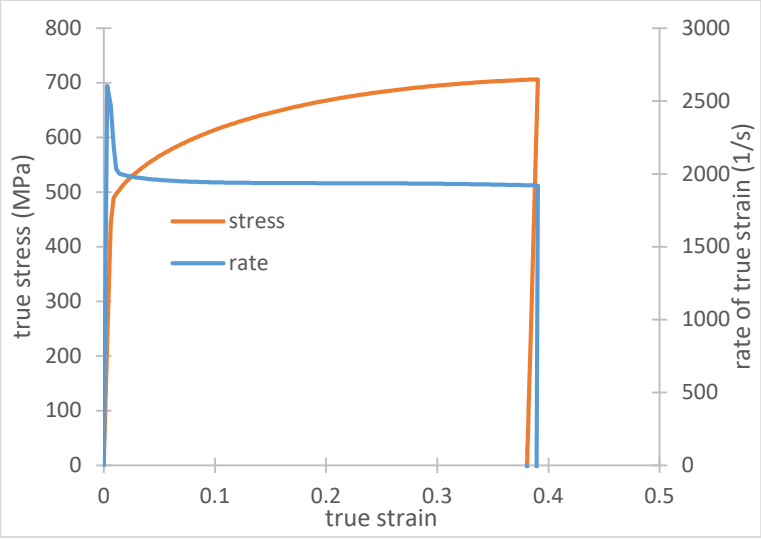

(b)

Fig. 6 (a) Strain signals for the steel bar (8000 kg/m^3), 500-mm-long striker at 27 m/s. (b) Stress–strain curve and strain rate; the rate is much more constant when the steel bar is used.

6.2 Example 2: Sample Recovery

In this example, the lab wants to recover a sample for postmortem examination. This means that the sample cannot be reloaded by later stress-wave reverberations in the bars. The intent is to have the sample loaded at a constant rate of 2000/s and unloaded at a final true strain of 0.2. The previous example showed that the steel bar maintains the desired strain rate better, so the steel bars are considered here. The final strain is reduced to 0.2 by using a shorter striker bar of 250 mm. Because the rate is largely constant, the striker length can simply be scaled from the previous example to achieve the desired final strain (250 mm = 500 mm × 0.2/0.4), but in a more complex situation it can be determined by varying the length of the striker iteratively until the final strain of 0.2 is achieved.

The predicted strain signals in this instance are shown in Fig. 7a, and the predicted stress–strain curve in Fig. 7b. The desired rate and final strain are achieved on the initial loading; however, the sample is reloaded when the reverberation of the reflected pulse reaches the sample. This can also be seen in Fig. 8, which plots u_1, u_2, and P_s as functions of time. The reloading occurs at about 1.2 ms.

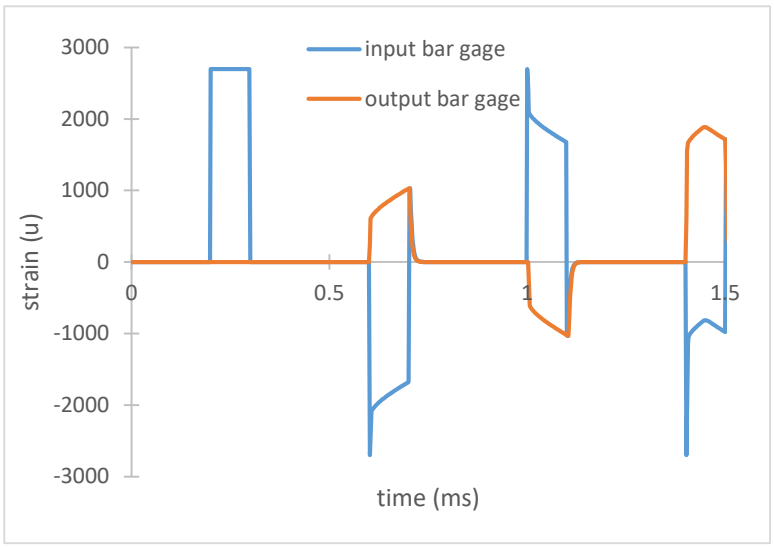

(a)

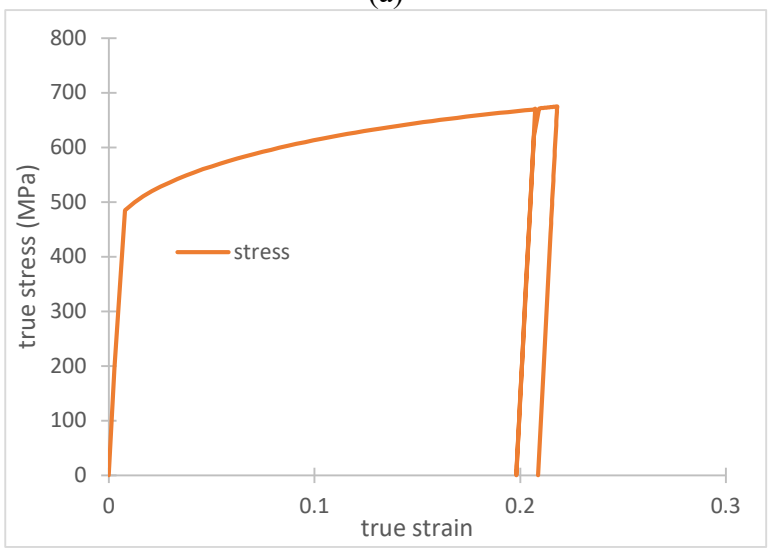

(b)

Fig. 7 Strain signals (a) and stress–strain curves when a 250-mm-long striker is used to limit sample deformation to a final strain of 0.2. The bars are steel. Note the sample is reloaded.

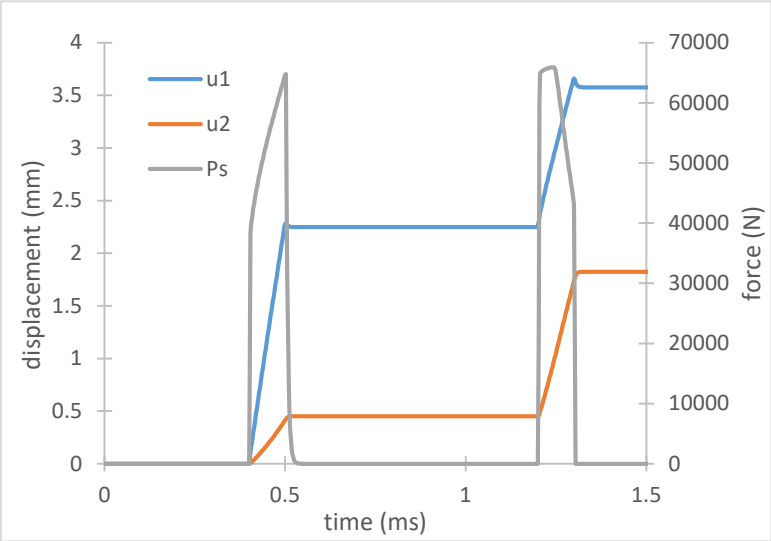

Fig. 8 Displacements u_1 and u_2 along with the force applied to the sample P_s plotted with time. The sample is reloaded at about 1.2 ms.

There are several ways to prevent the reloading. One of the easiest is to use a shorter output bar. This way, the motion of the bar end (u_2) associated with the reflection of the output pulse arriving at the sample will move the bar away from the input bar before the reflected pulse (i.e., the reflection of the reflected pulse from the input bar's striker face) arrives at the sample. This motion may be sufficient to prevent reloading, and can be calculated by the algorithm. Continuing the example, it is decided to use a 500-mm-long output bar instead of the normal 2000-mm output bar (perhaps the striker from the previous example). Strain gages are not mounted at the midpoint, but 100 mm from the sample to ensure the output pulse can be measured cleanly. These changes are made to the input table, and the strain signals, stress–strain curve, and displacement/sample load are plotted in Figs. 9a, 9b, and 10, respectively. Figures 9b and 10 show no evidence of reloading, and it can easily be shown that this is true for all larger times simply by carrying the simulation to a time where a clear pattern of steady-state reverberations are established showing u_2 increasing more rapidly than u_1. Under these conditions, it is impossible for the sample to be reloaded and the bar's long-term motion can be arrested in a variety of ways that will preserve the sample without additional damage.

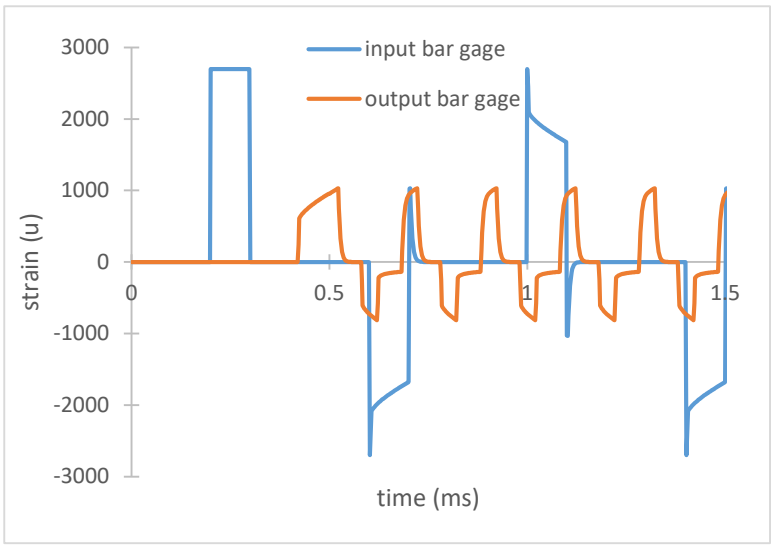

(a)

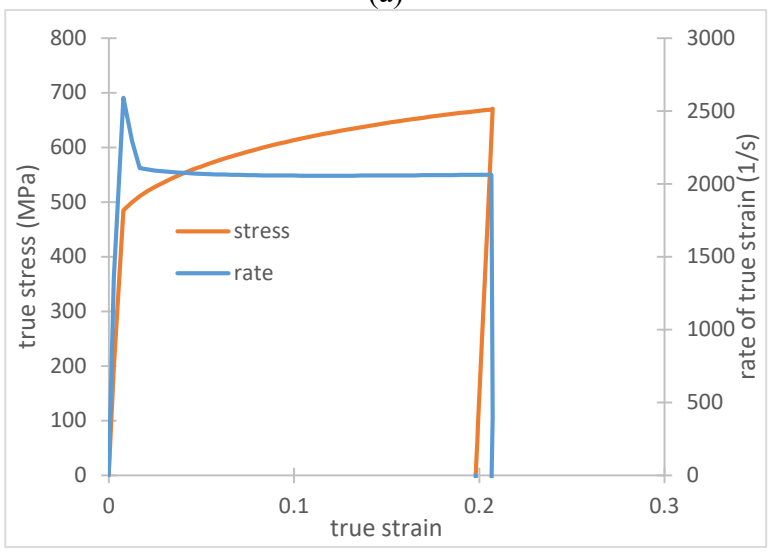

(b)

Fig. 9 (a) Strain signals and (b) stress–strain curve for a test when a 500-mm-long output bar is used. No reloading occurs.

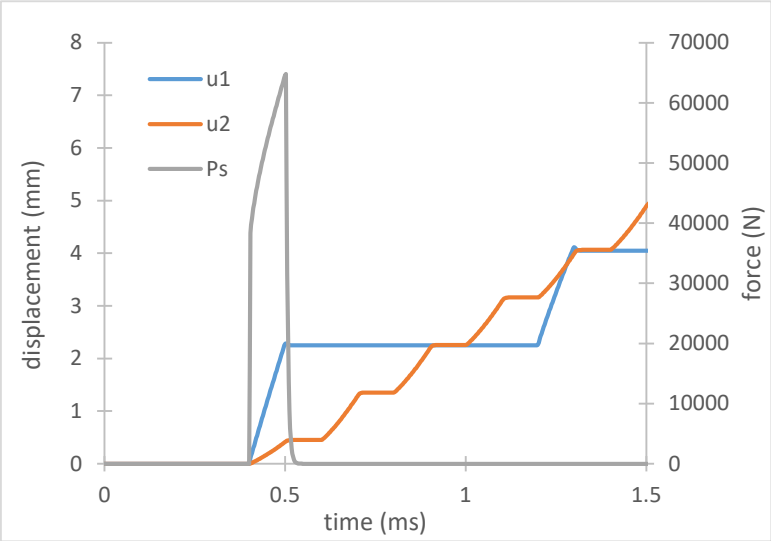

Fig. 10 Load and displacement of the bar ends when a 500-mm-long output bar is used. The output bar travels down range faster than the input bar does, so the sample is not reloaded due to later reflections in the bars.

6.3 Example 3: A Partial Unloading Cycle Using a Variable Impedance Striker

This final example demonstrates the design of a more complicated experiment. The application is high-rate spherical indentation.[15] It consists of a 450-mm-long aluminum input bar (3.18 mm diameter) and a 100-mm-long steel output bar (1.6 mm diameter). The indenter shape (R = 6.35 mm) is machined directly into the end of the output bar and has a negligible effect on its otherwise uniform impedance. A 6061-T6 aluminum sample is mounted to the end of the input bar, and the striker-impact drives the sample into the indenter. Indentation force and depth can be determined from a standard analysis. Although this is not a traditional specimen, the load versus indentation depth is approximately known from conventional (low-rate) indentation experiments,[16] so the sample behavior can be described by Eq. 23. The relevant properties are summarized in Table 2, and at this point the experiment is adequately represented by Fig. 3, and the equations discussed therein.

Table 2 Input properties for an indentation example

input bar			output bar			sample (eqns. 23 & 24)		
L =	406.4	*mm*	L =	100	*mm*	A =	0.05	*N*
d =	3.175	*mm*	d =	1.5875	*mm*	B =	1265000	N/mm^2
ρ =	2800	kg/m^3	ρ =	8000	kg/m^3	n =	0.05	*N*
c =	5000	*m/s*	c =	5000	*m/s*	k =	90000	N/mm

The complication in this example arises from the need to pulse shape. In some situations with indentation, it is of interest to partially unload and reload the sample during the test because this allows the contact area between the sample and the indenter to be estimated.[17] This is easily done with conventional indentation equipment, but is more difficult at high loading rates. One possible method is to use a striker whose impedance varies in such a way that the resulting input pulse temporarily decreases in magnitude so that the sample can partially unload (i.e., a tapered striker that is considerably thinner in the middle than at the ends). The question then becomes how to precisely design this striker bar.

It is possible (recall Eq. 5; see also Casem[10]) to determine the input pulse needed to apply a desired strain-rate history to a sample, including a partial unloading. It is then possible to solve for the projectile shape (approximately) needed to create such an input pulse; see Casem[10] and Liu and Li.[18] These are inverse techniques, and the resulting projectile shape may not be practical or even possible to make. They are also fairly complex to implement. An alternate approach is to treat the tapered striker as consisting of a finite number of uniform impedance segments (i.e., a "stepped" projectile instead of a true taper). The equations in Section 2 then apply to each segment, with boundary conditions at each end such that the force and velocity are continuous across the interfaces between adjacent segments. A further simplification can be made if the length of each segment is the same, so that the time needed for a wave to travel the length of each segment is identical. This leads to the method described by Bacon,[19] which lends itself particularly well to the trial and error approach to experiment design used here.

The Bacon method has been implemented into the algorithms presented previously using a 10-segment striker. The impedance of each segment is varied in a logical manner until the desired unloading is obtained in the predicted force versus indentation depth curve. In this way, Bacon's method provides $P_S(t)$ to the method described in Section 3. One possible projectile shape is shown in Fig. 11. The impact end is to the right, and the projectile is a high-strength aluminum alloy (assumed strong enough to remain elastic). The impedance (cross-sectional area) is varied by a changing the inner and outer diameter of the striker; some thought has been given as to how the striker will be machined and how it will be launched from a gas gun. These diameters are given in Table 3. With an impact speed of 5.5 m/s, the predicted strain gage signals are shown in Fig. 12a. The discrete steps in the input pulse are due to the segmentation of the bar; in a real experiment these would largely be absent due to dispersion. The dip in the middle of the pulse allows the sample to unload, and the partial unloading is shown in the predicted force versus indentation-depth curve (Fig. 12b).

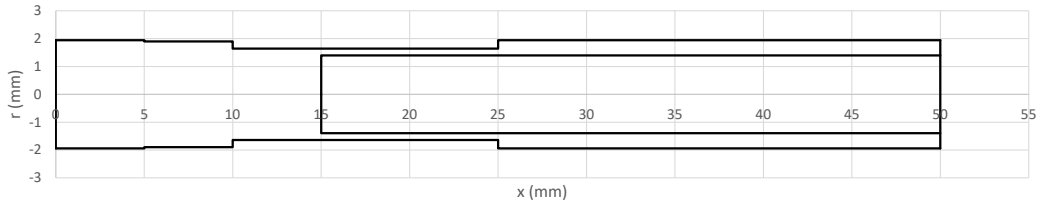

Fig. 11 A striker with a variable impedance used to create a partial unloading and reloading during a high-rate indentation experiment. The striker is axisymmetric; the "negative radius" is shown simply to aid in visualization.

Table 3 Geometry of the tapered striker that is input to the analysis (inner and outer diameters). Properties of aluminum are assumed (ρ = 2800 kg/m^3 and c = 5000 m/s). The total length is 50 mm, so each segment is 5 mm long.

segment #	1	2	3	4	5	6	7	8	9	10
d_i (mm)	0	0	0	2.794	2.794	2.794	2.794	2.794	2.794	2.794
d_o (mm)	3.886	3.8	3.284276	3.284276	3.284276	3.886	3.886	3.886	3.886	3.886
A (mm^2)	11.86029	11.34115	8.471672	2.340512	2.340512	5.729134	5.729134	5.729134	5.729134	5.729134

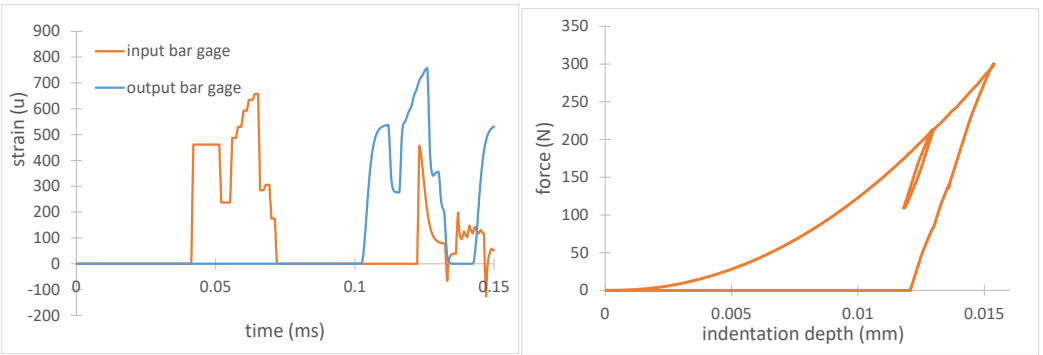

Fig. 12 (a) Strain-gage signals for an indentation experiment. (b) The oddly shaped input pulse is created by the variable impedance striker in Fig. 11, and leads to a partial unloading and reloading of the sample during the experiment.

7. Conclusion

The algorithms presented in this report are useful for designing Kolsky bar experiments. By using standard wave equation solutions and assuming a specimen behavior, any Kolsky bar experiment can be predicted in advance. This allows one to choose testing parameters such as sample size, bar material and geometry, and striker speed, to obtain a desired test. The Kolsky bar is used in many modified forms, and the methods discussed can be adapted to other experiments that have considerable complexity. The example of a variable impedance striker bar to

achieve a partial unloading cycle during indentation is given, but even more complex situations are possible. For example, Casem et al.[20] used a 1-D finite element simulation to design a tapered striker that when used with an elastic-plastic pulse shaper would be suitable for testing a linear elastic sample. This could easily have been done using the algorithms presented here, eliminating the need to use finite elements. Similarly, algorithms have been developed to predict the input pulse created by various pulse shaping methods (e.g., Frew et al.[21,22] and Forrestal and Warren[23]). These could be implemented as well, and the parameters therein included in the iterative scheme to design the pulse shaper.

Finally, in this work, the method was implemented in the commercial spreadsheet Microsoft Excel, and used as a trial-and-error approach. Test parameters are varied to achieve various changes in the final stress–strain curve to guide the experimentalist. This works well for users with some experience with Kolsky bar testing. However, they could easily be incorporated into numerical optimization schemes to handle more complex problems, or to find more optimum designs.

8. References

1. Kolsky H. An investigation of the mechanical properties of materials at very high rates of loading. Proc R Soc London. 1949;B62:676–700.
2. Follansbee PS. The Hopkinson bar, metals handbook. American Society for Metals. 1985;8(9):198–217.
3. Meyers M. Dynamic behavior of materials. Wiley; 1994. p. 305–310.
4. Gray GT 3rd. Classic split-Hopkinson pressure bar testing. In: Kuhn H, Medlin D, editors. Mechanical testing and evaluation, vol. 8. ASM International; 2002. p. 462–476.
5. Chen W, Song B. Split Hopkinson (Kolsky) bar, mechanical engineering series. Springer; 2011.
6. Gorham DA. A numerical method for the correction of dispersion in pressure bar signals. J Phys E Sci Instrum. 1983;16(6):477–479.
7. Follansbee PS, Franz C. Wave propagation in the split-Hopkinson pressure bar. J Eng Mat Tech. 1983;105:61.
8. Gong JC, Malvern LE, Jenkins DA. Dispersion investigation in the split-Hopkinson pressure bar. J Eng Mat Tech. 1990;112:309–314.
9. Bancroft D. The velocity of longitudinal waves in cylindrical bars. Phys Rev. 1941;59:588–593.
10. Casem DT. Hopkinson bar pulse-shaping with variable impedance projectiles-an inverse approach to projectile design. Army Research Laboratory (US); 2010. Report No. ARL-TR-5246.
11. Graff KF. Wave motion in elastic solids. Dover Publications; 1992.
12. Kolsky H. Stress waves in solids. Dover Publications; 1963.
13. Johnson G, Cook W. A constitutive model and data for materials subjected to large strains, high strain rates, and high temperatures. Proceedings of the 7th International Symposium on Ballistics; 1983; The Hague, Netherlands. p. 541–547.
14. Casem DT, Dandekar DP. Shock and mechanical response of 2139-T8 aluminum. J Appl Phys. 2012;111:063508.

15. Casem DT, Pittari JJ 3rd, Swab J. High-rate indentation using miniature Kolsky bar methods. In: Mates S, Eliasson V, Allison P, editors. Dynamic behavior of materials, volume 1. Conference Proceedings of the Society for Experimental Mechanics Series; 2021. Springer, Cham.

16. Fernandez-Zelaia P, Joseph VR, Kalidindi SR, Melkote SN. Estimating mechanical properties from spherical indentation using Bayesian approaches. Materials & Design. 2018;147:92–105.

17. Kalidindi SR, Pathak S. Determination of the effective zero-point and the extraction of spherical nanoindentation stress–strain curve. Acta Materialia. 2008;56:3523–3532.

18. Liu D, Li X. Dynamic inverse design and experimental study of impact pistons. Chinese J Mech Eng. 1998;34(4):506214.

19. Bacon C. Longitudinal impact of a shaped projectile on a Hopkinson bar. J App Mech. 1994;61:493–495.

20. Casem DT, Dwivedi AK, Swab JJ, Wright JC, Mondal AB. Analysis of a three-bar Kolsky apparatus for high-rate three point flexure, J Dynamic Behavior Mater. 2015;1:5–93.

21. Frew DJ, Forrestal MJ, Chen W. Pulse shaping techniques for testing elastic-plastic materials with a split Hopkinson pressure bar. Exp Mech. 2005;45:186–195.

22. Frew DJ, Forrestal MJ, Chen W. Pulse shaping techniques for testing brittle materials with a split Hopkinson pressure bar. Exp Mech. 2002;42:93–106.

23. Forrestal MJ, Warren TL. A conical striker bar to obtain constant true strain rate for Kolsky bar experiments. J Dynamic Behavior Mater. 2021;7:161–164. https://doi.org/10.1007/s40870-020-00269-1.

1 (PDF)	DEFENSE TECHNICAL INFORMATION CTR DTIC OCA
1 (PDF)	DEVCOM ARL FCDD RLD DCI TECH LIB
1 (PDF)	DEVCOM ARL FCDD RLW TC D CASEM